P. Oßwald, R. Whitside, J. Schäffer, M. Köhler, An experimental flow reactor study of the combustion kinetics of terpenoid jet fuel compounds: farnesane, p-menthane and p-cymene, Fuel 187 (2017) 43-50.

[doi 10.1016/j.fuel.2016.09.035]

An experimental flow reactor study of the combustion kinetics of terpenoid jet fuel compounds: farnesane, p-menthane and p-cymene

Patrick Oßwald[1], Ryan Whitside[1], Johannes Schäffer[2] and Markus Köhler[1]

[1]*Institute of Combustion Technology, German Aerospace Center (DLR), Pfaffenwaldring 38-40, D-70569 Stuttgart, Germany*

[2]*Department of Chemical Engineering, University of Bayreuth, Universitätsstraße 30, D-95440 Bayreuth, Germany*

Corresponding author: Markus Köhler
German Aerospace Center *(DLR)*
Pfaffenwaldring 38-40
D-70569 Stuttgart
Germany
FAX: +49 711 578
Email: m.koehler@dlr.de

Supplemental material has been included in the submission of this paper.

An experimental flow reactor study of the combustion kinetics of terpenoid jet fuel compounds: farnesane, p-menthane and p-cymene

Patrick Oßwald[1], Ryan Whitside[1], Johannes Schäffer[2] and Markus Köhler[1]

[1]*Institute of Combustion Technology, German Aerospace Center (DLR), Pfaffenwaldring 38-40, D-70569 Stuttgart, Germany*

[2]*Department of Chemical Engineering, University of Bayreuth, Universitätsstraße 30, D-95440 Bayreuth, Germany*

Abstract

The combustion kinetics of three bio jet fuel compounds farnesane, p-menthane and p-cymene, derived from natural terpenoids, have been investigated experimentally by an atmospheric high temperature flow reactor coupled with molecular beam mass spectrometric detection (MBMS). Quantitative speciation data for their oxidation chemistry in combustion is presented to provide an insight into the combustion behavior and provide detailed validation data for kinetic modeling. The experimental results are compared and discussed to analyze distinct combustion phenomena such as fuel consumption pathways and soot precursor chemistry.

The fuel selection focuses on biotechnologically producible terpenoid components, namely the isoalkane 2,6,10-trimethyl dodecane (farnesane), the cycloalkane 1-isopropyl-4-methylcyclohexane (p-menthane) and the branched aromatic compound 1-isopropyl-4-methylbenzene (p-cymene). Literature data on farnesane (recently approved with up to 10% blending in Jet A-1) is limited and even scarcer for the two potential synthetic fuel additive species, p-menthane and p-cymene. The comprehensive, systematic experimental speciation data set including the single fuel components for lean to rich stoichiometries (0.5 to 1.5) is available in the supplemental material to this contribution.

Keywords: Biofuels; jet fuel components; molecular beam mass spectrometry (MBMS); speciation; Flow reactor

1. Introduction

The development of aviation fuel has relied on the historical composition of fossil kerosene, putting restrictions on the requirements set out by organizations such as ASTM International or the European Committee for Standardization (CEN) [1, 2]. Future “fuel design” can allow aviation to move past these limitations, by combining new approaches in fuel logistics systems and engines, optimized for next generation fuels [2-4]. Biofuels also have the potential to remove aviation dependence on fossil fuels, offset CO_2 emissions and hopefully reduce other harmful pollutants such as soot and its toxic precursors [5]. Considering the current growth rate of air travel and the increase in overall CO_2 emissions over the next decades, biofuels are considered a feasible option to technically realize the ambitious goals committed to by the IATA. Among these are CO_2 neutral growth by 2020 and a net halving of carbon emissions by 2050 compared with 2005. Additionally, the European Commission (EC) launched its clean fuel strategy “Clean power for transport” including a comprehensive and vast European alternative fuels strategy in 2013. Here, a long term policy framework is envisioned for synthetic fuels substituting conventional jet fuels.

Even with this relatively newly explored subject, the approaches and strategies are already manifold and rapidly growing. An overview of biofuels in aviation is given by Blakey et al. [6] and Braun-Unkhoff et al. [7], showing the current certified alternative aviation fuels and strategies involved. Moreover, the challenges and obstacles in jet fuel design for the complex mixtures from various sources are discussed, ranging from HEFA (Hydrotreated Ester and Fatty Acid) and FT-SPK (Fischer-Tropsch Synthetic Paraffinic Kerosene) blends to the recently approved ATJ (Alcohol-to-Jet) [8]. However, the specific range of suitable alternative fuels is quite limited for usage in all existing aircraft. While synthetic paraffinic kerosenes (SPKs) from biological sources are widely expected to reduce CO_2 emissions, their combustion behavior is not yet fully understood and may lead to different pollutant-forming mechanisms and, consequently, new or different emission patterns [9, 10]. Dryer presented a comprehensive review on chemical kinetic and combustion characteristics of

transportation fuels in general, clearly demonstrating the challenges and potentials of current fuel design strategies and methods [3, 7]. Conclusively, strategies involving surrogate fuel mixtures are likely to succeed in delivering results on a reasonable timescale in this complex topic.

Further interest was gained after a single molecule passed ASTM tests and specifications (D7566, 3rd annex) as a drop-in fuel with up to 10 % to be added in Jet A-1. The approval of 2,6,10-trimethyl dodecane, also known as farnesane ($C_{15}H_{32}$), opens new pathways to characterization strategies and more focused investigations on synthetic jet fuels, in comparison to the very complex and variable mixtures of fuel components typically associated with alternative jet fuels [3]. Farnesane is a synthesized iso-paraffinic (SIP) fuel produced from hydroprocessed fermented sugars [11]. Production utilizes a fermentation process in which yeast, currently engineered by Amyris Biotechnologies, consumes sugar cane syrup to produce the terpene farnesene, which is then converted to farnesane through hydrogenation [11]. Farnesane has the potential to be more commercially viable compared to other biofuels because it is already being produced in an Amyris owned factory in Brazil, with a farnesene production capacity of 50 million liters per year. Subsequent conversion to farnesane has been measured at up to 99.7% efficiency.

Terpenoid compounds, also called isoprenoid, are the largest class of natural compounds, and with extremely diverse chemical and functional properties, they have great potential as alternative fuel in aviation [12-14]. High density renewable fuels can be synthesized via α-pinene, camphene, limonene, and crude turpentine [15].

In fact, the Amyris patent involving farnesane in aviation features jet fuel compositions including two other molecules, which may be produced from the biotechnologically accessible terpene, limonene [16]. These are the cycloalkane 1-isopropyl-4-methylcyclohexane (p-menthane, $C_{10}H_{20}$) and the aromatic species 1-isopropyl-4-methylbenzene (p-cymene, $C_{10}H_{14}$), see Fig. 1.

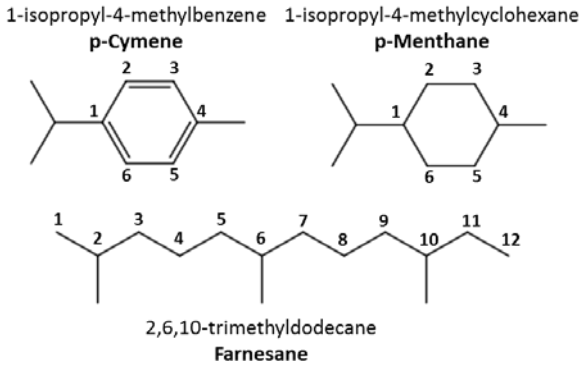

Figure 1: Chemical structures of the investigated jet fuel components.

p-Menthane can be similarly produced by hydrogenating other essential oils, such as terpenines, menthol and a variety of others including direct conversion from p-cymene itself [17]. Further investigation into the production of p-menthane from renewable materials, specifically for use as aviation fuel, was undertaken by Fraga et al. [18]. They focused on renewable production of cycloalkanes, which are typically found in crude-oil-derived fuels. Typically, cycloalkanes have low freezing points, high energy content, are resistant to oxidation and lack sulfur and nitrogen impurities. These properties make cycloalkanes [19] like p-menthane attractive for the replacement of carcinogenic aromatics in aviation fuels.

p-Cymene is of significant interest as a bio-renewable feedstock because it is already used in a wide variety of industrial processes [20]. Currently, commercial production of cymenes is from toluene and propylene, which are obtained from crude oil. There have also been studies for the production of renewable p-cymene using pinenes, limonene or eucalyptus oil as natural feedstock [17, 21]. The main interest in p-cymene would be as an additive to other aviation biofuels free of aromatic compounds such as Fischer-Tropsch fuels or HEFA fuels, since the current minimum aromatic content in aviation fuels is set to 8% for material compatibility.

Investigations on the combustion kinetics of the three molecules are, however, limited. For farnesane, only measurements of ignition delay times and extinction limits are available [22] while laminar flame speed [23] and effects of the substitution pattern on the low temperature oxidation [24] of cymene have been investigated.

Here, we present the first quantitative speciation data for the three terpenoid jet fuel candidates farnesane, p-menthane and p-cymene. The contribution provides quantitative species profiles from the DLR high temperature flow reactor coupled with MBMS detection [25] for the development and validation of combustion models. Such speciation flow reactor experiments have proven to be an excellent validation target for chemical kinetic models e.g. [26] with GC-detection, applied low pressure pyrolysis [27, 28] or even elevated pressures [29].

2. Experimental

The DLR high temperature flow reactor has been described in literature recently [25, 30], and is thus only briefly described here. The system consists of the high temperature laminar flow reactor, including gas supplies and vaporizer system and is coupled to a molecular beam mass spectrometry (MBMS) system. The reactor has an alumina (Al_2O_3) ceramic tube with 40 mm inner diameter and a total length of 1497 mm. The premixed laminar flowing gases are fed highly diluted (99% Ar) into the reactor to suppress heat release and a self-sustaining reaction. The dimensions of the reactor were chosen to minimize boundary effects by the relatively large reactor diameter.

The vaporizer of the system [25] was updated with a commercial setup (Bronkhorst, CEM) with a pneumatically driven fuel supply, now equipped with a Coriolis flow meter (Bronkhorst, Mini Cori-Flow M12) for precise control of the fuel mass flow rate. The gas inlet system consists of the vaporizer system alongside a preheated gas supply flow (80°C), premixing the gases prior to the reactor inlet. The gas flows are directly regulated by Coriolis mass flow meters of the same type. All supply lines with pre-vaporized fuels are preheated at 150°C (180°C for farnesane) to prevent condensation of the liquid fuels, while avoiding pyrolysis processes. Complete and stable vaporization was found to occur at temperatures below the boiling point of the respective fuels (i.e. 150°C for the C_{10}-fuels and 200°C for farnesane), while complete evaporation was ensured by the small fuel fraction and the low partial pressure (below 1 mbar) needed. Complete evaporation was

checked through vaporizer response speed to fuel shut-off. The premixed gases are fed into the reactor by a tempered flange equipped with a porous bronze plug to create homogeneous flow conditions.

The reaction segment has a total length of 1000 mm, heated by a customized high temperature oven (Gero, Type HTRH 40-1000) capable of temperatures up to 1900 K. Measurement series were performed at constant inlet flow conditions, while a monotonically decreasing (-200 K/h) oven temperature ramp was applied in the temperature between 900–1150°C. Note that the residence time is dependent on the respective oven temperature. Corresponding residence times range from around 2.1 s (1000 K) to 1.8 s (1200 K) for the given conditions.

The averaging time of each data point of the MBMS setup was chosen to correspond to a 2.5 K temperature interval. Note that careful characterization of the experimental setup with special focus on temperature behavior and uncertainties of the reactor is described elsewhere, including an approach for kinetic modeling [25]. Good agreement of experimental results with accepted chemical kinetic models is found, following the same approach successfully used in other reactor experiments [31, 32]. Finally, due to the temperature reproducibility, a relative precision of the measured temperatures of ±5 K or better can be stated for the present reactor experiment. Therefore, a scaling approach has been used to correct an experimental (thermocouple) temperature profile for the actual gas temperature with respect to a given oven temperature T_{Oven}. Effects like thermal inertia of the system or absolute offset are corrected by this scaling approach [25]. Note that some experimental constants of the scaling law have been updated for the present study.

Gases are sampled by a quartz cone at the centerline of the reactor exit at ambient pressures (laboratory is located at 460 m above sea level, corresponding to a mean pressure around 960 mbar). Sampling is centered at the end of the reaction zone, roughly 30 mm within the reactor exit via a 50 µm orifice at the quartz nozzle tip. The molecular beam is guided to the ion source of an electron impact (EI) time-of-flight mass spectrometer (Kaesdorf, mass resolution of R = 3000) and species are detected by their exact mass. The ionization energy was set to 11.5 eV (actual peak value of electron

energy distribution; FWHM 1.4 eV) in order to avoid fragmentation inside the ion source. The system's performance allows for the determination of the elemental composition (C/H/O) of stable and radical species present in the combustion process down to concentrations in the ppm regime.

2.3 Fuel synthesis and operating conditions

The proposed jet fuel compositions by Amyris consisting of the 3 terpenoid compounds farnesane ($C_{15}H_{32}$), p-cymene ($C_{10}H_{14}$) and p-menthane ($C_{10}H_{20}$) are measured for the 3 stoichiometries 0.5, 1.0 and 1.5. p-Cymene (≥ 99.5% in purity) was purchased from Sigma Aldrich, while farnesane (>98% in purity) and p-menthane (>96% in purity) were synthesized by the University of Bayreuth.

Farnesane is obtained from 80 ml farnesene (Sigma Aldrich) via hydrogenation with 0.6 g 5% Pd/C catalyst at 10 bar H_2 for 2 days around room temperature. p-Menthane is derived from 80 ml limonene (Sigma Aldrich) via hydrogenation with 1 g 5% Pd/C as catalyst at 25 bar H_2 and room temperature. Both products were filtered, distilled and analyzed by GC, GC-MS and ^{13}C-NMR.

Table 1 shows the applied flow conditions. Note the divergence in stoichiometry caused by zero point instability of the applied Coriolis flowmeter for the stoichiometric p-menthane and lean p-cymene, p-menthane series. Thus, an increased fuel flow has to be considered for the respective measurements. However, the deviation is small and does not affect the general interpretation of the dataset. Note that the reaction conditions were chosen to cover a wide range from lean, stoichiometric and rich conditions.

Table 1: Inlet flow conditions for the investigated fuels. An additional argon flow of 9.9 slm was added for dilution to all conditions.

Fuel	**Farnesane**			**p-Cymene**			**p-Menthane**		
Stoichiometry ϕ	0.5	1.0	1.5	0.6	1.1	1.5	0.6	1.0	1.5
Fuel (l) [mg/min]	20.2	39.5	58.1	25.4	45.3	59.9	24.2	39.1	56.9
Fuel (g) [sccm]	2.13	4.17	6.13	42.3	7.56	10	3.87	6.24	9.09
O2 [sccm]	97.9	95.8	93.9	96.4	93.1	90	96.8	93.8	90.9

2.4 Data evaluation and uncertainties

Quantitative data evaluation follows the well-established procedures of measurements for flames described in [33-36] and for reactor measurements [31, 37], so only a brief description is given here.

The integrated and corrected ion signal S of a specific species i is linked to its mole fraction x by comparison to the respective signal of a reference species (Ar). Signals have been corrected for background and, when necessary, for contributions of ^{13}C isomers. Even though soft ionization conditions (11.5 eV) were used, fragmentation in the ion source cannot be avoided completely. Thus, signal corrections for fragment ions of the fuel and intermediate species have been applied, when fragmentation has been observed during the calibration measurements. This correction is, however, small for stable species, but may be significant for radical species with low concertation. The electron-energy-dependent calibration factor $k_{i/R}(E)$ for the individual species is constituted from experimental constants:

$$\frac{S_i}{S_{Ar}} = \frac{x_i}{x_{Ar}} \cdot k_{i/Ar}(E) \quad (1)$$

From the given equation, the mole fractions are calculated with argon as the reference species. Its mole fraction can be assumed as constant due to the high dilution of the reactant gases (x_{Ar} = 99%).

Major species (product, reactant) are calibrated by direct cold gas measurements except for H_2O, where an internal calibration strategy relying on the H- and O-balances (depending on the stoichiometry) was used to obtain a calibration factor. Calibration factors for the intermediate species presented herein are obtained by the "Direct" or "RICS" method, depending on the respective species. Stable and commercially available species are calibrated directly by cold gas measurements. The RICS method (relative ionization cross section) [38] based on the measurement of electron ionization efficiency curves of chemically similar reference species is used for evaluation. Statistical and relative uncertainties typical for MBMS signals are below 10 % [25, 30] as the standard deviation for poor signal-to-noise ratios is around 10 %. Therefore, a relative comparison of each species from different measurements offers high precision. Absolute uncertainty is highly dependent on the individual calibration of the distinct species, ranging from 15-20% for direct (cold gas) calibrated and major species, up to uncertainties in the order of factors 2-4 when ionization cross sections for non-direct calibrated intermediates species (RICS) have to be estimated. In total, the C and O atom balances deviate from the inlet composition by less than 10% for all measured product

compositions. This rises to a maximum of 30% at rich conditions at temperatures around 1000°C, where most intermediates peak. Note that the H balance is not conclusive in all cases, since no H_2 was measured due to the low ionization energy. The supplemental material provides a comprehensive list of the calibration data used for each species and the applied calibration method.

3. Results and discussion

Here, we present the first speciation data on combustion of the aforementioned terpenoid jet fuel compounds farnesane, p-menthane and p-cymene. To the best of our knowledge no kinetic models are currently available for the investigated fuels and thus the following analysis of the reaction system is only guided by the experimental results. The complete quantitative dataset on the experimental results is provided for development of detailed kinetic models and is available for download as supplemental material in a MS Excel data file. To enable kinetic modeling, temperature profiles are also added to the file. Additional information on quantification, temperature analysis and a suitable modeling approach can be found in [25].

3.1 Major species

Measured major species profiles, i.e. reactant and product species, plotted as a function of the flow reactor temperature for the three terpenoid fuels are summarized in Fig. 2. Results are obtained at ambient pressure for a constant premixed inlet flow and reflect the global combustion properties of the three fuels at lean (ϕ = 0.5), stoichiometric (ϕ =1.0) and rich (ϕ= 1.5) conditions.

The reaction sequence follows the structure typically seen for this type of flow reactor study [25, 31]: constant (inlet) composition is measured until first fuel consumption is observed at a certain temperature. First fuel consumption is typically observed prior to significant O_2 consumption and the fuel is primarily converted to combustion intermediates. With increasing temperature, the reactivity of the system is increased until a sufficient radical pool is established and rapid conversion of the present species occurs along with major O_2 consumption and CO oxidation. Even though no self-sustaining reaction occurs, this can be interpreted as ignition [25, 31]. Note that for the given highly diluted conditions, heat release is found to be negligible.

For all of the investigated fuels, this ignition temperature (i.e. the temperature with the steepest decrease of oxygen) increases with stoichiometry as commonly observed [25]. For rich conditions, the transition from intermediates to combustion products is observed over a wider temperature range compared to leaner mixtures and oxygen consumption exhibits a less steep slope.

p-Menthane shows similar ignition behavior with respect to the temperature of O_2 consumption. However, the fuel destruction is observed at slightly higher temperatures than for farnesane resulting in a slightly smaller temperature interval.

p-Cymene ignition can be observed at slightly higher temperatures compared to the aliphatic fuels. Again, fuel decay at all stoichiometries starts somewhat later than observed for farnesane. This is related to the enhanced stability of aromatic six membered ring, present in this fuel.

For all fuels complete conversion to CO_2 for lean and almost for stoichiometric conditions can be observed. The varied yield of CO_2 and H_2O reflects the different C/H ratio of the fuel molecules. For rich conditions, similar levels of CO are present in the product composition for all fuels. Note that a distinct amount of acetylene (C_2H_2) and diacetylene (C_4H_2) is present in the product gas. Investigations of very rich conditions have shown that these species decompose at around 1600 K after passing a plateau [30].

Conclusively, the findings for the trends with varying stoichiometry from lean to rich conditions and the main species profiles show typical behavior in terms of hydrocarbon oxidation chemistry for the investigated conditions. A comparison with earlier investigations (including e.g. CH_4 and C_2H_4) at similar conditions exhibit the same trends, which are also correctly predicted and proved by well-established chemical models (GRI 3.0, USC-II), see [25, 30].

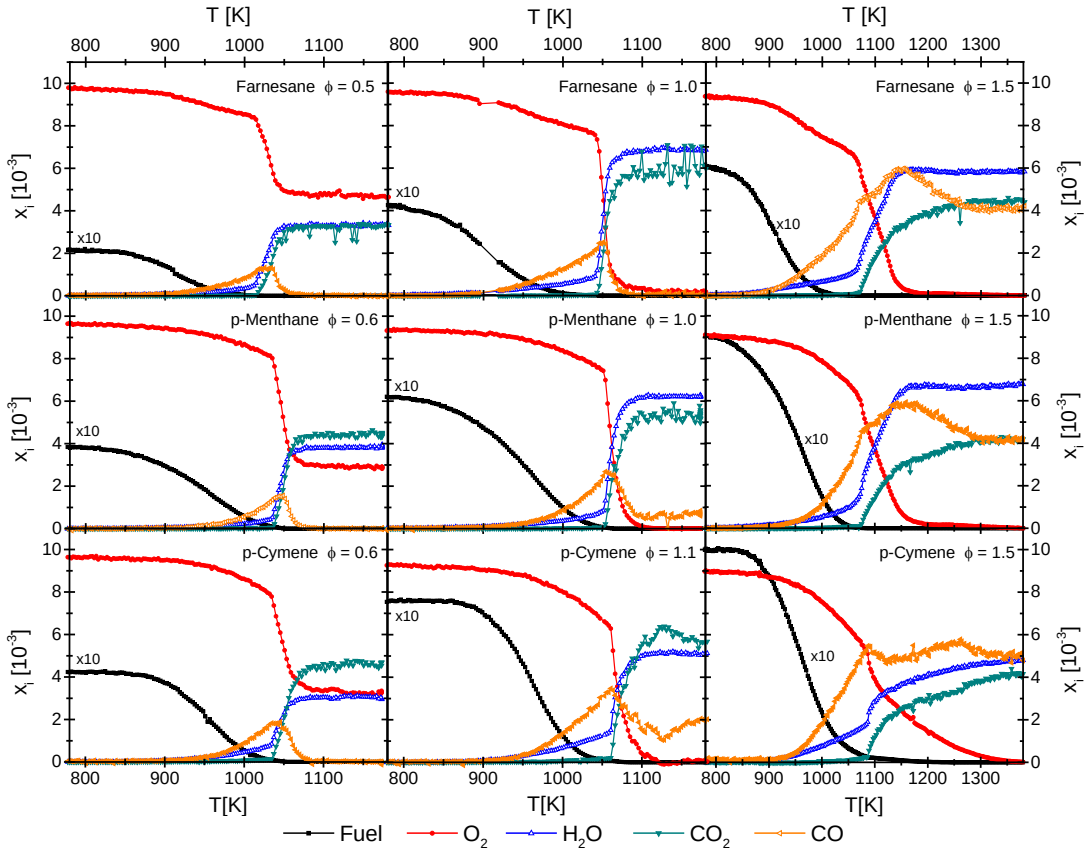

Figure 2: Mole fraction profiles for major species for various stoichiometries of farnesane, p-menthane and p-cymene are shown.

3.2 Intermediates

The stoichiometry dependence of combustion intermediates is presented in Fig. 3, utilizing the typical small combustion intermediates formaldehyde (CH_2O) and ethylene (C_2H_4). Effects due to varying stoichiometry are quite similar for all fuels. Conclusively, this indicates that all intermediates typically exhibit higher mole fractions at richer conditions due to the higher carbon content of the respective operating condition. A steep decay is seen at the stoichiometric and lean operating conditions caused by the rapid increase of reactivity when ignition occurs. For rich conditions, the decay edge is less sharp in agreement with the findings for the major species.

In general, a significantly lower concentration of small combustion intermediates is seen for the aromatic compound compared to the aliphatic fuels. This corresponds well with an increased amount of PAHs and soot precursors (sec. 3.4). Comparable concentrations of formaldehyde and other

oxygenated intermediates are detected for both aliphatic fuels. However, a slightly lower ethylene concentration is found for the cycloalkane.

All trends and ratios between fuels are similar for all stoichiometries, thus only stoichiometric operating conditions are compared in the following discussion on fuel decomposition and soot precursors. Profiles for all stoichiometries are available as electronic supplement.

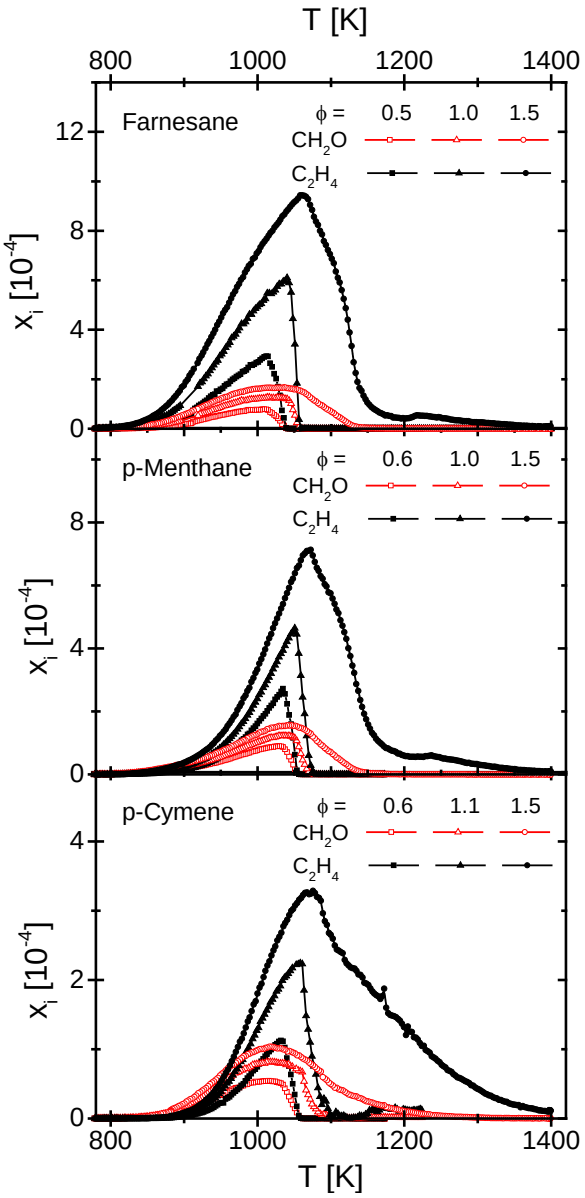

Figure 3: Intermediate mole fraction profiles for formaldehyde (CH_2O) and ethylene (C_2H_4) are shown for various stoichiometries.

3.3 Fuel decomposition

Fuel decomposition pathways may be derived from the sequence of peak temperatures of the respective intermediate profiles [25]. Figure 4 summarizes selected profiles of stable combustion intermediates originating from H-abstraction and subsequent β-scission of a C-H or C-C bond and shows the possible fuel decomposition pathways. The reaction chains (R1 or R2) are typically initiated by the attack of a reactive H or OH radical:

$$R\text{-}CH_2\text{-}CH_2\text{-}R' + H/OH \rightarrow R\text{-}\dot{C}H\text{-}CH_2\text{-}R' + H_2/H_2O \rightarrow R\text{-}CH{=}CH\text{-}R' + {}^{\cdot}H \quad (R1)$$

$$\rightarrow R\text{-}CH{=}CH_2 + {}^{\cdot}R' \quad (R2)$$

With R, R' being any hydrocarbon chain or H. Comparisons to smaller ($<C_4$) alkenes and acetylene are additionally provided. The selection of C_2H_2, C_2H_4, C_3H_6 and C_4H_8 is intentionally chosen for each fuel component to provide a basis for better comparison, while scission products are selected depending on the fuel. The smaller ($<C_4$) species can be produced from numerous reactions and are typically found downstream of the reaction pathways. They are typically found during the combustion of all hydrocarbons [39] and can even be built up from smaller molecules e.g. at rich methane combustion [40]. Since absolute concentrations vary by several orders of magnitude, profiles are scaled for comparison. Note, in contrast to C_2H_4 similar C_2H_2 concentrations are detected for all fuels, and as such C_2H_2 was set as the reference for the mole fraction axis.

In the present experiment, no information on the molecular structure was achievable. Therefore, all structures discussed below rely on plausibility considerations and more powerful techniques such as PEPICO [34] must be applied to determine a specific structure. The lowest peak temperature for farnesane, and subsequently the first intermediate, was found for $C_{15}H_{30}$ (not shown). This species may be formed from the fuel by H-abstraction and scission of any C-H bond forming a respective C_{15}-alkene. Thus, a mixture of several isomers can be expected. However, the determined mole fraction is very low ($3 \cdot 10^{-7}$, 3 orders of magnitude below propene) indicating only minor importance of this destruction pathway.

30 K above the C_{15}-alkenes, the products of several C-C scission channels shows their peak value. For example, $C_{14}H_{28}$ and $C_{13}H_{26}$ as products of the scission of a methyl or ethyl group of farnesane are measured. The potential mechanism of the elimination may be initial abstraction of a H-atom (by H, OH etc.), followed by the C-C bond scission in β-position or vice versa: The initial monomolecular C-C scission followed by the elimination of the respective H-atom, in order to form the double bond. However, based on the peak mole fractions of $C_{14}H_{28}$ and $C_{13}H_{26}$, the elimination of a CH_3 group is clearly favored. Even more noteworthy is the highest mole fraction among the first scission products to be found for $C_{10}H_{20}$ and C_9H_{18}, originating from the scission of the C-C bond between the 5th and 6th carbon atom or between the 4^{th} and 5^{th} carbon atom respectively (see Fig. 1). This finding indicates the formation of a double carbon bond after H-abstraction position at the 6^{th} carbon, resulting in a stable tertiary carbon radical as expected. Note that the respective scission counter products C_6H_{13} and C_5H_{11} are found as well at the same temperatures in concentrations of the order of 10^{-6} (not shown).

Other consecutive scission products butane (C_4H_8), propene (C_3H_6) and ethylene (C_2H_4) are determined with increasing peak temperatures, leading finally to C_2H_2 as the smallest unsaturated intermediate. In general, the fuel decomposition of farnesane follows very well the conventional hydrocarbon chemistry behavior.

For p-menthane oxidation, the C-H scission products peak at the lowest temperature. The respective $C_{10}H_{18}$ alkenes exhibit significantly higher concentrations than seen for the oxidation of the isoalkane farnesane. This indicates a higher importance of the H-elimination channel that is most likely favored by the less flexible ring structure of p-menthane.

Again 30 K above $C_{10}H_{18}$, the peak concentrations of C_9H_{16} and C_7H_{12} are reached. Both intermediates may be produced by loss of the methyl or isopropyl group of the fuel. Consequently, a substituted cyclohexene (methyl or isopropyl) can be expected as the identity of C_9H_{16} and C_7H_{12}. A further 45 K higher, C_6H_8 peaks, possibly as cyclohexadiene produced from subsequent loss of the second moiety.

For p-menthane, a similar consecutive order of smaller intermediates from butene to acetylene is seen comparably to the farnesane fuel. Note that the amount of butane produced from p-menthane is significantly below the value measured from farnesane oxidation.

For p-cymene, as for the other fuels, the lowest peak temperature is seen for the respective alkene ($C_{10}H_{12}$). Since abstraction from the aromatic core structure is less efficient [41], the double bond is expected to be formed at the isopropyl group to form p-cymenene (1-methyl-4-(1-methylethenyl)-benzene). Very high mole fractions are seen for C_9H_{10}, which may be the consecutive product from methyl loss by scission of CH_3 from the fuel or exchange of CH_3 by H of $C_{10}H_{12}$. Interestingly, propene exhibits its peak at the same temperature. The peak temperature is seen even prior to those of butene and other higher molecular species, clearly pointing to a reaction route fundamentally different from that seen for the aliphatic fuels. A reaction process like substitution of the isopropyl group of the fuel (eg. by H) at the aromatic ring may explain this finding. Due to the lower mole fraction of butene and other C_4-species, speculation on a buildup reaction pathway starting from propene is also plausible.

Moreover, high C_8H_8 mole fractions around $5 \cdot 10^{-5}$ are found for the p-cymene fuel decomposition chemistry, indicating a similar behavior to the recent report of Bierkandt et al. [42] with their closer investigation on the decomposition pathways of xylene in low-pressure flames. The C_8H_8 isomerization of benzocyclobutene to styrene is likely to be linked to the formation of indane and indene [43], both found here as well in high concentrations and are discussed in the following section. Furthermore, ring contractions to five-membered ring species like 1,3-cyclopentadiene (C_5H_6) are found similarly with maximum mole fractions of $2 \cdot 10^{-5}$ (not shown here) following the patterns in hydrocarbon chemistry discussed in [42]. However, for distinct identification and separation of the C_8H_8 or C_5H_6 isomers mentioned, more powerful techniques such as the PEPICO experiment are needed to gain a deeper insight into the isomerization processes.

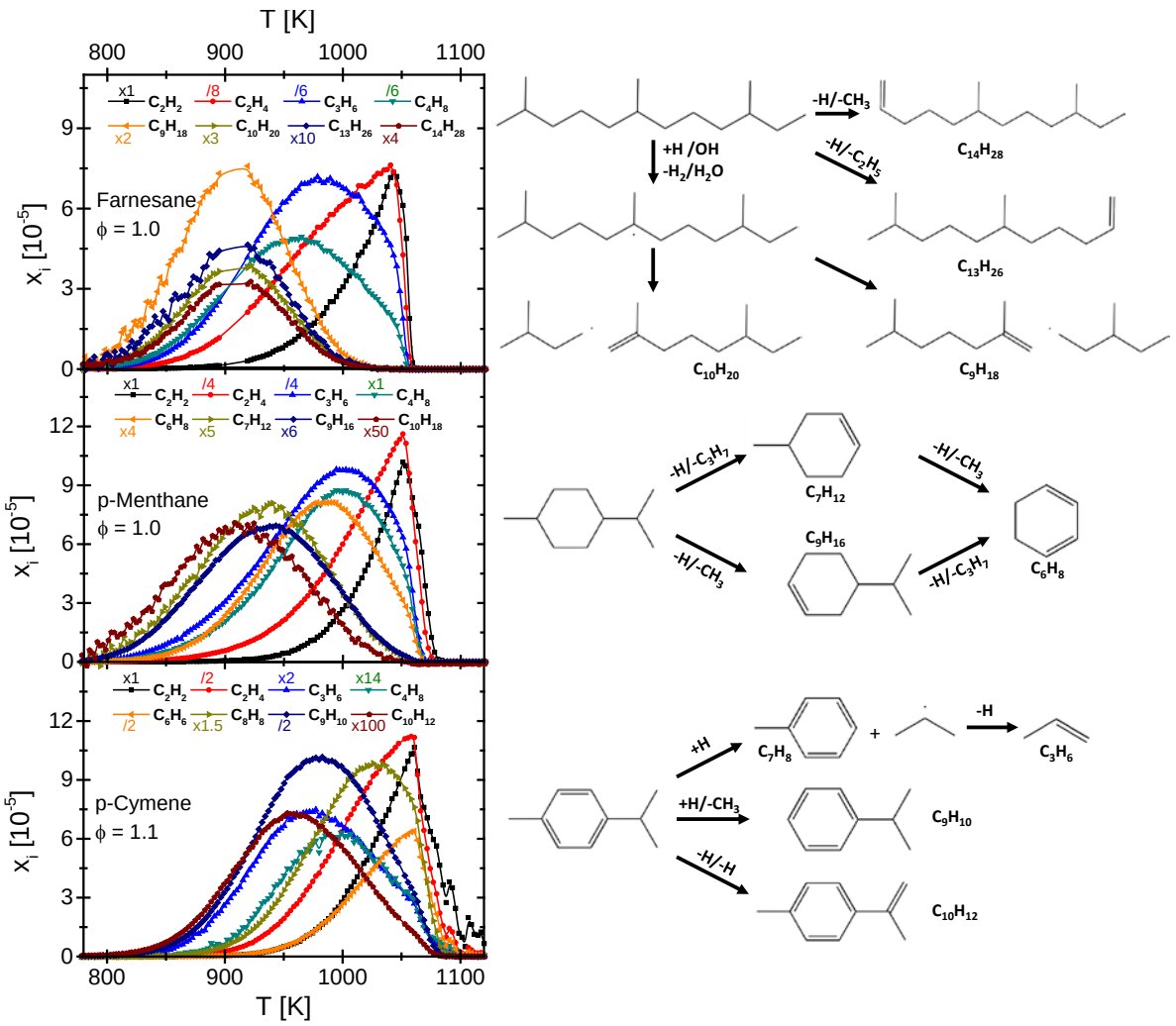

Figure 4: Left: Mole fraction profiles of selected intermediates occurring in the oxidation of farnesane, p-menthane and p-cymene. Profiles are scaled to acetylene for comparison. Right: Possible fuel decomposition pathways.

3.4 Soot precursors

Typical soot precursors (from propargyl to naphthalene) are summarized in Fig. 5. Propargyl (C_3H_3) and C_4H_5-species (main isomers CH_3CCCH_2, CH_3CHCCH and i-C_4H_5 [44]) are known to be benzene precursors. Especially C_3H_3 recombination reactions play a major role in benzene formation in many flames of aliphatic and oxygenated fuels [39]. This also seems to hold for the aliphatic fuels investigated herein. Due to the general low concentration of C_4H_5, the propargyl route of benzene formation is expected to be favored for all three fuels.

The aromatic p-cymene fuel exhibits the lowest concentrations of benzene precursors along with the highest measured benzene mole fraction among the measured fuels. Consequently, benzene formation can be expected directly from the fuel. Also, the ratio of benzene peak mole fractions between the three fuels (i.e. p-cymene > p-menthane > farnesane) is not conserved, when higher PAHs are considered. The formation of the phenyl radical on the other hand is clearly related to benzene, rather than to a radical recombination route, since it is only detected in noticeable concentrations for p-cymene.

Figure 5 shows the representative C_9H_8 (likely indene) and $C_{10}H_8$ (likely naphthalene) profiles, which exhibit about 10 times higher concentrations for p-cymene than in the p-menthane or even the farnesane fueled conditions. Regarding larger (>C_8) aromatic hydrocarbons for p-cymene combustion, a structured sequence of C_8H_8, C_8H_{10}, C_9H_8, C_9H_{10} $C_{10}H_8$, $C_{11}H_{10}$, $C_{11}H_{12}$, $C_{11}H_{14}$, $C_{12}H_8$, $C_{12}H_{10}$, $C_{12}H_{12}$ is observed up to m/z = 210. This sequence of higher PAHs is expected for aromatic combustion [42] and is also consistent with the high concentrations of C_8H_8 mentioned above for p-cymene, indicating a direct formation route to the known soot precursors indene ($7 \cdot 10^{-6}$) and indane ($1 \cdot 10^{-5}$) (not shown here). Thus, the p-cymene dataset is also well suited for validation of PAH growth mechanisms.

Finally one can consider that PAH formation and consequently the expected sooting behavior is not strictly coupled to the first aromatic ring formation as this is often the bottleneck of higher PAH formation in hydrocarbon combustion chemistry. As also seen for other aliphatic or oxygenated fuels [10], the soot precursor formation is highly dependent on the molecular structure of the fuel.

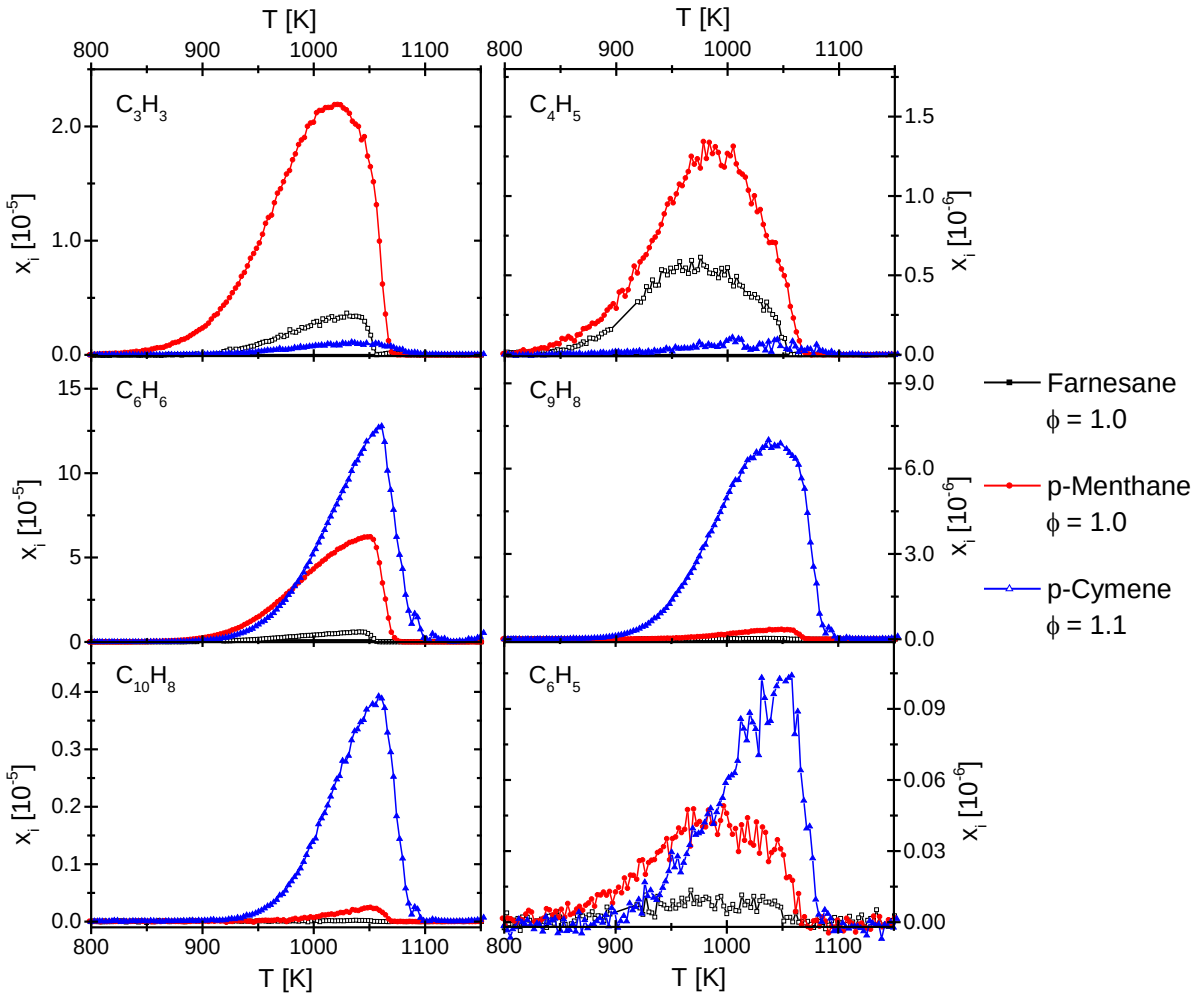

Figure 5: Mole fraction profiles of intermediate species related to the soot precursor chemistry obtained from the ϕ = 1.0 conditions.

4. Summary and conclusions

Quantitative speciation data for the approved jet fuel additive farnesane and two synthetic jet fuel candidate species p-menthane and p-cymene is presented and discussed alongside selected experimental species profiles. Although the three components may appear random at first glance, they share the same terpene-based organic feedstock and show great potential as alternative surrogates in aviation with respect to current fuel design strategies.

The comprehensive experimental data set presented here was obtained from the DLR high temperature flow reactor with coupled MBMS-TOF detection at atmospheric conditions. The

quantitative major and intermediate species mole fractions are presented for three stoichiometries and potential fuel decomposition and sooting reaction pathways are discussed. In particular, p-cymene is found to produce significantly more PAHs (indene, naphthalene or respective isomers), while this behavior appears not strictly coupled to the first aromatic ring formation (i.e. benzene). For the aromatic fuel p-cymene consecutive PAH structures up to m/z = 210 are reported and may also serve to validate PAH growth. In contrast, the combustion of farnesane shows very little to no tendencies to produce soot precursors.

The provided first speciation data on combustion for farnesane, p-cymene and p-menthane provides crucial data for the development and validation of combustion models, which will serve to evaluate the necessary properties of fuel mixtures designed for aviation. The full speciation data on the experimental results is available for download as supplemental material.

Acknowledgements:

The authors wish to thank the Helmholtz Energy-Alliance “Synthetic Liquid Hydrocarbons” and DLR CoE “Alternative Fuels” for financial support. P. Le Clercq and U. Riedel are gratefully acknowledged for discussions on alternative fuels in aviation.

References

[1] Annual book of ASTM Standards, 5.01–5.05, ASTM International, West Conshohocken PA., 2014.
[2] R. Parker, M. Lathoud, Green aero-engines: Technology to mitigate aviation impact on environment, Proc. Inst. Mech. Eng. C J. Mech. Eng. Sci., 224 (2010) 529-538.
[3] F.L. Dryer, Chemical kinetic and combustion characteristics of transportation fuels, Proc. Combust. Inst., 35 (2015) 117-144.
[4] L. Rye, C. Wilson, The influence of alternative fuel composition on gas turbine ignition performance, Fuel, 96 (2012) 277-283.
[5] International Air Transport Association, Report on Alternative Fuels, IATA, 2013.
[6] S. Blakey, L. Rye, C.W. Wilson, Aviation gas turbine alternative fuels: A review, Proc. Combust. Inst., 33 (2011) 2863-2885.
[7] M. Braun-Unkhoff, T. Kathrotia, B. Rauch, U. Riedel, About the interaction between composition and performance of alternative jet fuels, CEAS Aeronaut J, 7 (2016) 83-94.
[8] ASTM D7566-15b, Standard Specification for Aviation Turbine Fuel Containing Synthesized Hydrocarbons, ASTM International, West Conshohocken, PA, 2015.
[9] E.G. Giakoumis, C.D. Rakopoulos, A.M. Dimaratos, D.C. Rakopoulos, Exhaust emissions of diesel engines operating under transient conditions with biodiesel fuel blends, Prog. Energy Combust. Sci., 38 (2012) 691-715.
[10] K. Kohse-Höinghaus, P. Oßwald, T.A. Cool, T. Kasper, N. Hansen, F. Qi, C.K. Westbrook, P.R. Westmoreland, Cover Picture: Biofuel Combustion Chemistry: From Ethanol to Biodiesel (Angew. Chem. Int. Ed. 21/2010), Angew. Chem. Int. Ed., 49 (2010) 3545-3545.
[11] N.S. Renninger and D.J. McPhee. Fuel compositions comprising farnesane and farnesane derivatives and method of making and using same, July 15 2008. US Patent 7399323.
[12] B.G. Harvey, M.E. Wright, R.L. Quintana, High-Density Renewable Fuels Based on the Selective Dimerization of Pinenes, Energy Fuels, 24 (2010) 267-273.
[13] M.A. Rude, A. Schirmer, New microbial fuels: a biotech perspective, Curr. Opin. Microbiol., 12 (2009) 274-281.
[14] C. Vickers, J.Y.H. Behrendorff, M. Bongers, T.R. Brennan, M. Bruschi, L. Nielsen, Production of Industrially Relevant Isoprenoid Compounds in Engineered Microbes, in: B. Kamm (Ed.) Microorganisms in Biorefineries, Springer Berlin Heidelberg, 2015, pp. 303-334.
[15] H.A. Meylemans, R.L. Quintana, B.G. Harvey, Efficient conversion of pure and mixed terpene feedstocks to high density fuels, Fuel, 97 (2012) 560-568.
[16] Ryder, J.A., Jet fuel compositions, Sept. 15 200p. US Patent 7589243 B1, 2009.
[17] B.A. Leita, A.C. Warden, N. Burke, M.S. O'Shea, D. Trimm, Production of p-cymene and hydrogen from a bio-renewable feedstock-1,8-cineole (eucalyptus oil), Green Chemistry, 12 (2010) 70-76.
[18] M. A. Fraga, L. E. P. Borges, and F. Dos Reis Gonçalves. Catalytic hydrogenation of hydroxycycloalkanes and use of the product in biofuel compositions for aviation, May 23 2013. US Patent 20130131407.
[19] Z. Wang, L. Zhao, Y. Wang, H. Bian, L. Zhang, F. Zhang, Y. Li, S.M. Sarathy, F. Qi, Kinetics of ethylcyclohexane pyrolysis and oxidation: An experimental and detailed kinetic modeling study, Combust. Flame, 162 (2015) 2873-2892.
[20] T.P. Troy, M.J.Y. Tayebjee, K. Nauta, S.H. Kable, T.W. Schmidt, Atmospheric oxidation intermediates: Laser spectroscopy of resonance-stabilized radicals from p-cymene, Chem. Phys. Lett., 620 (2015) 129-133.
[21] M.A. Martín-Luengo, M. Yates, M.J.M. Domingo, B. Casal, M. Iglesias, M. Esteban, E. Ruiz-Hitzky, Synthesis of p-cymene from limonene, a renewable feedstock, Applied Catalysis B-environmental, 81 (2008) 218-224.
[22] S.H. Won, S. Dooley, P.S. Veloo, H. Wang, M.A. Oehlschlaeger, F.L. Dryer, Y. Ju, The combustion properties of 2,6,10-trimethyl dodecane and a chemical functional group analysis, Combust. Flame, 161 (2014) 826-834.

[23] K. Chetehouna, L. Courty, C. Mounaïm-Rousselle, F. Halter, J.-P. Garo, Combustion Characteristics of p-Cymene Possibly Involved in Accelerating Forest Fires, Combust. Sci. Technol., 185 (2013) 1295-1305.
[24] B. Rotavera, A.M. Scheer, H. Huang, D.L. Osborn, C.A. Taatjes, Influence of temperature and resonance-stabilization on the ortho-effect in cymene oxidation, Proc. Combust. Inst., 35 (2015) 543-552.
[25] P. Oßwald, M. Köhler, An atmospheric pressure high-temperature laminar flow reactor for investigation of combustion and related gas phase reaction systems, Rev. Sci. Instrum., 86 (2015) 105109.
[26] K.M. Van Geem, S.P. Pyl, G.B. Marin, M.R. Harper, W.H. Green, Accurate High-Temperature Reaction Networks for Alternative Fuels: Butanol Isomers, Industrial & Engineering Chemistry Research, 49 (2010) 10399-10420.
[27] L. Zhang, J. Cai, T. Zhang, F. Qi, Kinetic modeling study of toluene pyrolysis at low pressure, Combust. Flame, 157 (2010) 1686-1697.
[28] T. Zhang, J. Wang, T. Yuan, X. Hong, L. Zhang, F. Qi, Pyrolysis of methyl tert-butyl ether (MTBE). 1. Experimental study with molecular-beam mass spectrometry and tunable synchrotron VUV photoionization, J. Phys. Chem. A, 112 (2008) 10487-10494.
[29] C.C. Schmidt, C.T. Bowman, Flow reactor study of the effect of pressure on the thermal de-NOx process, Combust. Flame, 127 (2001) 1958-1970.
[30] M. Köhler, P. Oßwald, H. Xu, T. Kathrotia, C. Hasse, U. Riedel, Speciation data for fuel-rich methane oxy-combustion and reforming under prototypical partial oxidation conditions, Chem. Eng. Sci., 139 (2016) 249-260.
[31] F. Herrmann, P. Oßwald, K. Kohse-Höinghaus, Mass spectrometric investigation of the low-temperature dimethyl ether oxidation in an atmospheric pressure laminar flow reactor, Proc. Combust. Inst., 34 (2013) 771-778.
[32] Y. Li, L. Zhang, Z. Wang, L. Ye, J. Cai, Z. Cheng, F. Qi, Experimental and kinetic modeling study of tetralin pyrolysis at low pressure, Proc. Combust. Inst., 34 (2013) 1739-1748.
[33] P. Oßwald, H. Güldenberg, K. Kohse-Höinghaus, B. Yang, T. Yuan, F. Qi, Combustion of butanol isomers – A detailed molecular beam mass spectrometry investigation of their flame chemistry, Combust. Flame, 158 (2011) 2-15.
[34] P. Oßwald, P. Hemberger, T. Bierkandt, E. Akyildiz, M. Köhler, A. Bodi, T. Gerber, T. Kasper, In situ flame chemistry tracing by imaging photoelectron photoion coincidence spectroscopy, Rev. Sci. Instrum., 85 (2014) 025101.
[35] M. Schenk, L. Leon, K. Moshammer, P. Oßwald, T. Zeuch, L. Seidel, F. Mauss, K. Kohse-Höinghaus, Detailed mass spectrometric and modeling study of isomeric butene flames, Combust. Flame, 160 (2013) 487-503.
[36] P. Oßwald, K. Kohse-Höinghaus, U. Struckmeier, T. Zeuch, L. Seidel, L. Leon, F. Mauss, Combustion Chemistry of the Butane Isomers in Premixed Low-Pressure Flames, Z. Phys. Chem., 225 (2011) 1029-1054.
[37] F. Herrmann, B. Jochim, P. Oßwald, L. Cai, H. Pitsch, K. Kohse-Höinghaus, Experimental and numerical low-temperature oxidation study of ethanol and dimethyl ether, Combust. Flame, 161 (2014) 384-397.
[38] J.C. Biordi, Molecular beam mass spectrometry for studying the fundamental chemistry of flames, Prog. Energy Combust. Sci., 3 (1977) 151-173.
[39] N. Hansen, T.A. Cool, P.R. Westmoreland, K. Kohse-Höinghaus, Recent contributions of flame-sampling molecular-beam mass spectrometry to a fundamental understanding of combustion chemistry, Prog. Energy Combust. Sci., 35 (2009) 168-191.
[40] M. Köhler, P. Oßwald, H.-B. Xu, T. Kathrotia, C. Hasse, U. Riedel, Speciation data for fuel-rich methane oxy-combustion and reforming under prototypical partial oxidation conditions, Chem. Eng. Sci., 139 (2016) 249-260.

[41] W. Yuan, Y. Li, P. Dagaut, J. Yang, F. Qi, Experimental and kinetic modeling study of styrene combustion, Combust. Flame, 162 (2015) 1868-1883.
[42] T. Bierkandt, P. Hemberger, P. Oßwald, M. Köhler, T. Kasper, Insights in m-xylene decomposition under fuel-rich conditions by imaging photoelectron photoion coincidence spectroscopy Proc. Combust. Inst., (2016, accepted.).
[43] Y. Di, C.S. Cheung, Z. Huang, Comparison of the effect of biodiesel-diesel and ethanol-diesel on the gaseous emission of a direct-injection diesel engine, Atmos. Environ., 43 (2009) 2721-2730.
[44] N. Hansen, S.J. Klippenstein, C.A. Taatjes, J.A. Miller, J. Wang, T.A. Cool, B. Yang, R. Yang, L. Wei, C. Huang, J. Wang, F. Qi, M.E. Law, P.R. Westmoreland, Identification and Chemistry of C4H3 and C4H5 Isomers in Fuel-Rich Flames, The Journal of Physical Chemistry A, 110 (2006) 3670-3678.